Zhang, Jian-Bo; Bowman, Patrick Oswald; Leinweber, Derek Bruce; Williams, Anthony Gordon; Bonnet, Frédéric D. R.; CSSM Lattice Collaboration

http://hdl.handle.net/2440/18066

Scaling behavior of the overlap quark propagator in the Landau gauge

Jianbo Zhang,[1] Patrick O. Bowman,[1,2] Derek B. Leinweber,[1] and Anthony G. Williams[1]

[1]*Special Research Center for the Subatomic Structure of Matter (CSSM) and Department of Physics, University of Adelaide,*
5005, Australia
[2]*Nuclear Theory Center, Indiana University, Bloomington, Indiana 47405, USA*

Frédéric D. R. Bonnet

University of Regina, Department of Physics, University of Regina, Regina, Saskatchewan S4S 0A2, Canada

(CSSM Lattice Collaboration)

The properties of the momentum space quark propagator in Landau gauge are examined for the overlap quark action in quenched lattice QCD. Numerical calculations are done on three lattices with different lattice spacings and similar physical volumes to explore the approach of the quark propagator toward the continuum limit. We have calculated the nonperturbative momentum-dependent wave-function renormalization function $Z(\zeta^2;p)$ and the nonperturbative mass function $M(p)$ for a variety of bare quark masses and perform an extrapolation to the chiral limit. We find the behavior of $Z(\zeta^2;p)$ and $M(p)$ are in reasonable agreement between the two finer lattices in the chiral limit, however the data suggest that an even finer lattice is desirable. The large momentum behavior is examined to determine the quark condensate.

I. INTRODUCTION

The quark propagator is one of the fundamental quantities in QCD. By studying the momentum-dependent quark mass function in the infrared region we can gain valuable insight into the mechanism of dynamical chiral symmetry breaking and the associated dynamical generation of mass. There have been several studies of the momentum space quark propagator [1–9] in Landau gauge using different fermion actions. Here we focus on the overlap fermion action and extend previous work [8] to three lattices with different lattice spacing a at fixed physical volume. This allows us to study the approach of the Landau gauge quark propagator to the continuum limit. The study of the overlap quark propagator in the Gribov copy-free Laplacian gauge is underway and will be reported elsewhere.

II. QUARK PROPAGATOR ON THE LATTICE

In a covariant gauge in the continuum, the renormalized Euclidean space quark propagator has the form

$$S(\zeta^2;p) = \frac{1}{i\not{p}A(\zeta^2;p^2) + B(\zeta^2;p^2)} = \frac{Z(\zeta^2;p^2)}{i\not{p} + M(p^2)}, \quad (1)$$

where ζ is the renormalization point. The renormalization point boundary conditions for $M(p^2)$ and $Z(\zeta,p^2)$ are chosen to be

$$Z(\zeta^2;\zeta^2) \equiv 1, \quad M(\zeta^2) \equiv m(\zeta^2). \quad (2)$$

where, at sufficiently large renormalization point ζ, $m(\zeta^2)$ is the usual renormalized (running) quark mass. The functions $A(\zeta^2;p^2)$ and $B(\zeta^2;p^2)$, or alternatively $Z(\zeta^2;p^2)$ and $M(p^2)$, contain all of the nonperturbative information of the quark propagator. Note that $M(p^2)$ is renormalization point

independent, i.e., since $S(\zeta^2;p)$ is multiplicatively renormalizable all of the renormalization-point dependence is carried by $Z(\zeta^2;p^2)$. For sufficiently large momenta, the effects of dynamical chiral symmetry breaking become negligible, i.e., for large p^2, and we have $M(p^2) \rightarrow m(\zeta)$ up to logarithmic corrections, where $m(\zeta)$ is the perturbative running mass.

When all interactions for the quarks are turned off, i.e., when the gluon field vanishes (or the links are set to one), the quark propagator has its tree-level form

$$S^{(0)}(p) = \frac{1}{i\not{p} + m^0}, \quad (3)$$

where m^0 is the bare quark mass. When the interactions with the gluon field are turned on we have

$$S^{(0)}(p) \rightarrow S^{\text{bare}}(a;p) = Z_2(\zeta^2;a)S(\zeta^2;p), \quad (4)$$

where a is the regularization parameter—in this case, the lattice spacing—and $Z_2(\zeta^2;a)$ is the quark wave-function renormalization constant chosen so as to ensure $Z(\zeta^2;p^2) = 1$. For simplicity of notation we suppress the a-dependence of the bare quantities.

On the lattice we expect the bare quark propagators, in momentum space, to have a similar form as in the continuum, except that the $O(4)$ invariance is replaced by a four-dimensional hypercubic symmetry on an isotropic lattice. Hence, the inverse lattice bare quark propagator takes the general form

$$(S^{\text{bare}})^{-1}(p) \equiv i\left(\sum_\mu C_\mu(p)\gamma_\mu \right) + B(p). \quad (5)$$

We use periodic boundary conditions in the spatial directions and antiperiodic in the time direction. The discrete momentum values for a lattice of size $N_i^3 \times N_t$, with $n_i = 1, \ldots, N_i$ and $n_t = 1, \ldots, N_t$, are

$$p_i = \frac{2\pi}{N_i a}\left(n_i - \frac{N_i}{2}\right), \quad \text{and} \quad p_t = \frac{2\pi}{N_t a}\left(N_t - \frac{1}{2} - \frac{N_t}{2}\right). \tag{6}$$

The overlap fermion formalism [10,11] realizes an exact chiral symmetry on the lattice and is automatically $\mathcal{O}(a)$ improved. The massive overlap operator can be written as [12]

$$D(\mu) = \frac{1}{2}[1 + \mu + (1 - \mu)\gamma_5 \epsilon(H_w)], \tag{7}$$

where $H_w(x,y) = \gamma_5 D_w(x,y)$ is the Hermitian–Wilson-Dirac operator, the mean-field improved Wilson-Dirac operator can be written as

$$\begin{aligned}D_w(x,y) &= [(-m_w a) + 4r]\delta_{x,y} - \frac{1}{2}\sum_\mu \{(r - \gamma_\mu) \\ &\quad \times U_\mu(x)\delta_{y,x+\hat\mu} + (r + \gamma_\mu)U_\mu^\dagger(x - a\hat\mu)\delta_{y,x-\hat\mu}\} \\ &= \frac{u_0}{2\kappa}\left[\delta_{x,y} - \kappa\sum_\mu \left\{(r - \gamma_\mu)\frac{U_\mu(x)}{u_0}\delta_{y,x+\hat\mu}\right. \right. \\ &\quad \left.\left. + (r + \gamma_\mu)\frac{U_\mu^\dagger(x - a\hat\mu)}{u_0}\delta_{y,x-\hat\mu}\right\}\right]. \end{aligned} \tag{8}$$

The negative Wilson mass $(-m_w a)$ is then related to κ by

$$\kappa \equiv \frac{u_0}{2(-m_w a) + (1/\kappa_c)}, \tag{9}$$

and mean-field improvement allows the use of the tree-level value $\kappa_c = 1/(8r)$. The Wilson parameter is typically chosen to be $r = 1$, and we will also use $r = 1$ here in our numerical simulations. The dimensionless quark mass parameter is

$$\mu \equiv \frac{m^0}{2m_w}. \tag{10}$$

The overlap quark propagator is given by the equation

$$S^{\text{bare}}(m^0) \equiv \tilde{D}_c^{-1}(\mu), \tag{11}$$

where

$$\tilde{D}_c^{-1}(\mu) \equiv \frac{1}{2m_w}\tilde{D}^{-1}(\mu)$$

and

$$\tilde{D}^{-1}(\mu) \equiv \frac{1}{1 - \mu}[D^{-1}(\mu) - 1]. \tag{12}$$

At tree-level, the inverse bare lattice quark propagator becomes the tree-level version of [Eq. (5)]

$$(S^{(0)})^{-1}(p) \equiv i\left(\sum_\mu C_\mu^{(0)}(p)\gamma_\mu\right) + B^{(0)}(p). \tag{13}$$

We calculate $S^{(0)}(p)$ directly by setting the links to unity in the coordinate space quark propagator and taking its Fourier transform. It is then possible to identify the appropriate kinematic lattice momentum directly from the definition

$$q_\mu \equiv C_\mu^{(0)}(p) \tag{14}$$

The form of $q_\mu(p_\mu)$ is shown and its analytic form given in Ref. [8]. Having identified the appropriate kinematical lattice momentum q, we can now define the bare lattice propagator as

$$S^{\text{bare}}(p) \equiv \frac{Z(p)}{i\slashed{q} + M(p)}. \tag{15}$$

This ensures that the free lattice propagator is identical to the free continuum propagator. Due to asymptotic freedom the lattice propagator will also approach the continuum form at large momentum. In the gauge sector, this analysis approach dramatically improves the gluon propagator [13,14].

The two Lorentz invariants can now be [24]

$$Z^{-1}(p) = \frac{1}{12iq^2}\text{Tr}\{\slashed{q}S^{-1}(p)\} \tag{16}$$

$$M(p) = \frac{Z(p)}{12}\text{Tr}\{S^{-1}(p)\}. \tag{17}$$

While Z is directly dependent on our choice of momentum q, the mass function M is indirectly dependent on this choice. In the case of staggered quarks it has been seen that the kinematic momentum derived from tree-level analysis of the action is a good choice of momentum for the mass function [5,6]. This is an empirical result. The tree-level behavior of the Overlap quark propagator is rather different, however, and a different approach may be needed. We investigate this issue by analyzing the scaling behavior of the propagator over three values of the lattice spacing at constant physical volume.

III. NUMERICAL RESULTS

We present results from three lattice ensembles, each with a different lattice spacing a, but having the same physical volume. Lattice parameters are summarized in Table I. The gauge configurations were created using a tadpole improved plaquette plus rectangle (Lüscher-Weisz [15]) gauge action. Each ensemble consists of 50 configurations. The lattice spacing was determined by the static quark potential using the string tension $\sqrt{\sigma} = 440$ MeV [16].

The gauge field configurations were gauge-fixed to the $\mathcal{O}(a^2)$ improved Landau gauge [17]. Our calculation begins with the evaluation of the inverse of the Dirac operator in Eq. (7). We approximate the matrix sign function $\epsilon(H_w)$ by a 14th-order Zolotarev approximation [18]. The coordinate space propagator, Eq. (11), is calculated for each configura-

TABLE I. Lattice parameters.

Action	Volume	N_{Therm}	N_{Samp}	β	a (fm)	u_0	Physical volume (fm^4)
Improved	$16^3 \times 32$	5000	500	4.80	0.093	0.89650	$1.5^3 \times 3.00$
Improved	$12^3 \times 24$	5000	500	4.60	0.123	0.88888	$1.5^3 \times 3.00$
Improved	$8^3 \times 16$	5000	500	4.286	0.190	0.87209	$1.5^3 \times 3.00$

tion. A discrete Fourier transform is then applied to the each of the coordinate space propagators, and the momentum-space bare quark propagator $S^{\text{bare}}(p)$ is finally obtained from the ensemble average.

In the Wilson action we use $\kappa = 0.19163$ for the regulator mass. We calculate the Overlap quark propagator for ten quark masses on each ensemble by using a shifted Conjugate Gradient solver. The quark mass parameter μ was adjusted to make the tree-level bare quark mass in physical units, the same on three lattices. For example, we choose $\mu = 0.018$, 0.021, 0.024, 0.030, 0.036, 0.045, 0.060, 0.075, 0.090, and 0.105 on ensemble 1, i.e., the $16^3 \times 32$ lattice with $a = 0.093$ fm. This corresponds to bare masses in physical units of $m^0 = 2\mu m_w = 127$, 148, 169, 211, 254, 317, 423, 529, 634, and 740 MeV, respectively.

Results from ensemble 2 were presented in Ref. [8], and some results from ensemble 3 were also reported in Ref. [9]. Here we will compare the quark propagators on each ensemble to examine its behavior as the lattice spacing vanishes. First we present some results from ensemble 1, the finest lattice of the three. All data has been cylinder cut [13]. Statistical uncertainties are estimated via a second-order, single-elimination jackknife.

In Fig. 1 we show the results for all ten masses for both the mass and wave-function renormalization functions, $M(p)$ and $Z^{(R)}(p) \equiv Z(\zeta^2; p)$, respectively, as a function of the discrete lattice momentum p. $Z^{(R)}(p)$ is renormalized at $\zeta = 3.44$ GeV. We see that both $M(p)$ and $Z^{(R)}(p)$ are reasonably well behaved up to 5 GeV. In the plots of $M(p)$ the data is ordered as one would expect by the values for μ, i.e., the larger the bare quark mass m^0, the higher is the $M(p)$ curve. At small bare masses $M(p)$ falls off more rapidly with momentum, which is understood from the fact that a larger proportion of the infrared mass is due to dynamical chiral symmetry breaking at small quark masses. In the nonrelativistic limit, the mass function would be a constant.

$Z^{(R)}(p)$ on the other hand is infrared suppressed. The smaller the quark mass, the more pronounced the dip at low momenta. This behavior is qualitatively consistent with what is seen in Dyson-Schwinger-based QCD models [19,20]. It is likely that some of the suppression, however, is due to the finite volume [6]. In Fig. 2 we repeat these plots but now using the kinematical lattice momentum q. This only alters the large momentum behavior of the propagator.

We perform an extrapolation to zero quark mass by a linear fit to the data. At sufficiently large momenta the mass function will be proportional to the bare quark mass, in which case the linear extrapolation is appropriate. Nonlinear behavior is to be expected in the infrared, but this simple ansatz describes the present data adequately. In the ultraviolet, the renormalized Z should—and does—approach its per-

turbative value of 1. This is mass independent. We investigated the effect of including the smallest quark masses in the chiral extrapolation and found that eliminating the lightest two made little difference to the extrapolated result. The resulting estimate of the chiral limit is shown in Fig. 3. These are shown against both p and q, renormalized as before. We see that both $M(p)$ and $Z^{(R)}(p)$ deviate strongly from their tree-level behavior. In particular, as in earlier studies of the Landau gauge quark propagator [3–5,8], we find a clear signal of dynamical mass generation and a significant infrared suppression of the $Z^{(R)}(p)$ function. At the most infrared point—the lowest nonzero momentum available on this lattice—the dynamically generated mass has the value
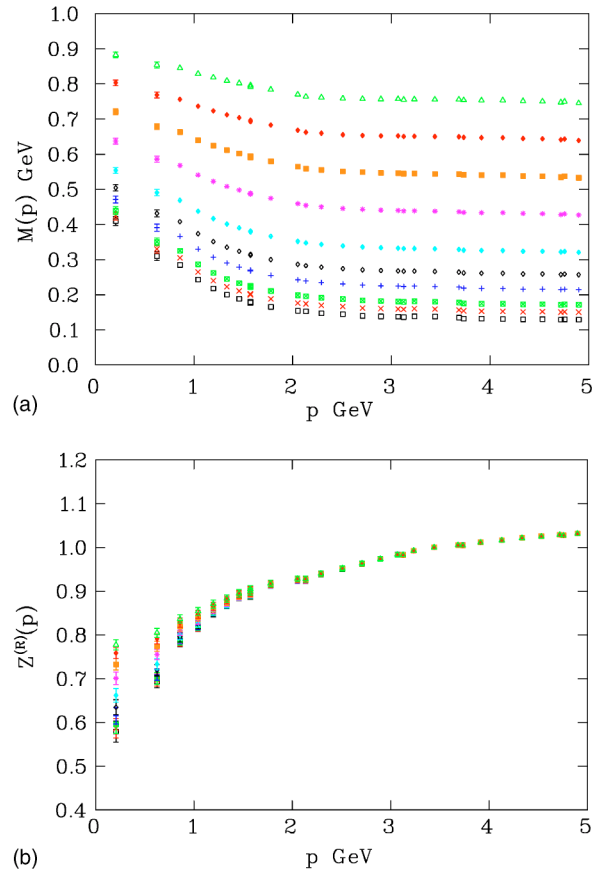

(a)

(b)

FIG. 1. The functions $M(p)$ and $Z^{(R)}(p) \equiv Z(\zeta^2; p)$ renormalized at $\zeta = 3.44$ GeV for all ten quark masses. Data are plotted versus the discrete momentum values defined in Eq. (6), $p = \sqrt{\Sigma p_\mu^2}$, over the interval [0,5] GeV. The data correspond to bare quark masses (from bottom to top) $\mu = 0.018$, 0.021, 0.024, 0.030, 0.036, 0.045, 0.060, 0.075, 0.090, and 0.105, which in physical units correspond to $m^0 = 2\mu m_w \simeq 127$, 148, 169, 211, 254, 317, 423, 529, 634, and 740 MeV, respectively.
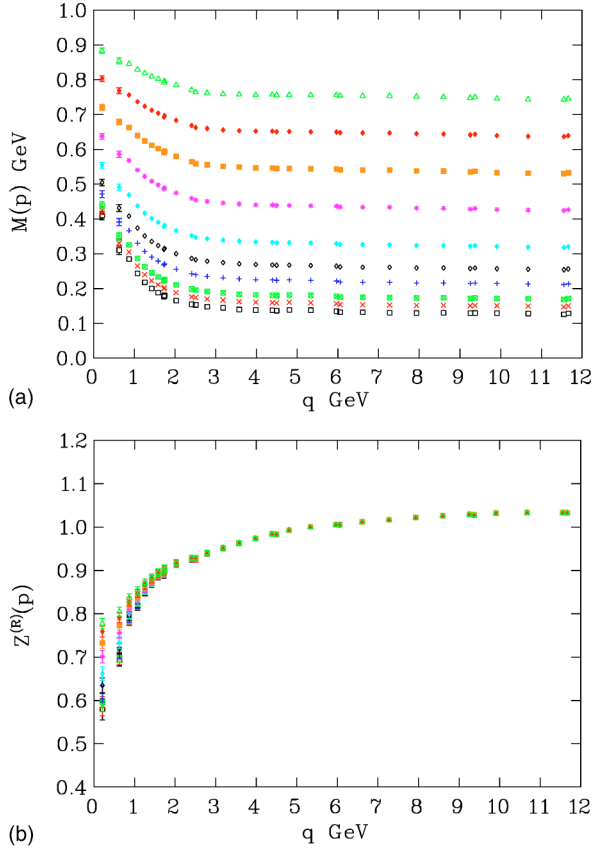
FIG. 2. The functions $M(p)$ and $Z^{(R)}(p) \equiv Z(\zeta^2;p)$ for renormalization point $\zeta = 5.31$ GeV for all ten quark masses. Data are shown versus the discrete momentum values defined in Eq. (14), $q = \sqrt{\Sigma q_\mu^2}$, over the interval $[0,12]$ GeV. The data in both parts of the figure correspond from bottom to top to increasing quark masses. The values of the bare quark masses are in the caption of Fig. 1.

$M_{IR} = 307(6)$ MeV and the momentum-dependent wave-function renormalization function has the value $Z_{IR} = 0.55(2)$. These values are very similar to the results found in previous studies [3–6,8] and are also similar to typical values in QCD-inspired Dyson-Schwinger equation models [19,20]. The results of Ref. [6] suggests that at least some of the infrared suppression of $Z^{(R)}(p)$ is due to finite volume effects.

Now we present the results on three lattices for comparison. These lattices have approximately the same physical volume, but each has a different lattice spacing. Thus we can study the Overlap propagator's scaling properties. We present the results for the chiral limit. The mass function, $M(p)$ for the three lattices in the chiral limit is plotted in Fig. 4, using both p and q. We see that if the mass function $M(p)$ is plotted against the standard lattice momentum p, the agreement of the results among the three lattices is better than the case in which the mass function $M(p)$ is plotted against kinematical lattice momentum q.

The results for the renormalization function $Z^{(R)}(p) \equiv Z(\zeta^2;p)$ of the three lattices is plotted in Fig. 5. Here the renormalization points are chosen to be $\zeta = 3.44$ GeV in p scale and $\zeta = 5.31$ GeV in q scale. Contrary to the case of
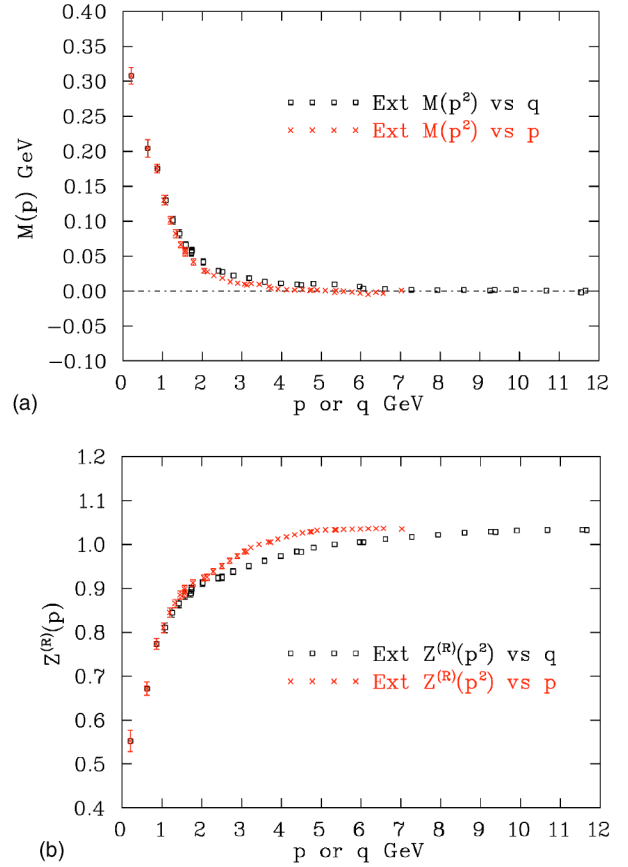

FIG. 3. Linearly extrapolated estimates of $M(p)$ and $Z^{(R)}(p) \equiv Z(\zeta^2;p)$ in the chiral limit. Here the renormalization point are $\zeta = 3.44$ GeV in the p scale and $\zeta = 5.31$ GeV in the q scale. At the smallest accessible momentum $M_{IR} = 307(6)$ MeV and $Z_{IR} = 0.55(2)$.

mass function $M(p)$, but as predicted by the tree-level analysis, the agreement between the results on three lattices is better if $Z^{(R)}(p)$ is plotted against the kinematical lattice momentum q. There are also the relatively small discrepancies in $Z^{(R)}(p)$ versus q in the infrared region on three lattices; it seems that in the continuum limit, the dip in the renormalization function $Z^{(R)}(p)$ will be narrow, but the depth of the dip will be unchanged. It suggests that an even finer lattice will be needed to confirm the continuum limit of $Z^{(R)}(p)$ in the infrared. It is possible that the linear chiral extrapolation is unreliable for $Z^{(R)}(p)$ in this regime or it could be that dynamical chiral symmetry breaking is coupling hypercubic lattice artifacts to finite volume effects. This warrants further investigation with finer and larger lattices.

Thus we have resolved one of the key questions raised in the studies of Ref. [8]. We see that the continuum limit appears to be approached most rapidly when $Z^{(R)}(p)$ is plotted against q and $M(p)$ is plotted against p. The better scaling of $Z^{(R)}(p)$ as a function of q is natural and predicted by the tree-level analysis. That $M(p)$ is better against p is purely observation.

Another way of studying scaling is by making comparisons with known continuum results. In the chiral limit, in the
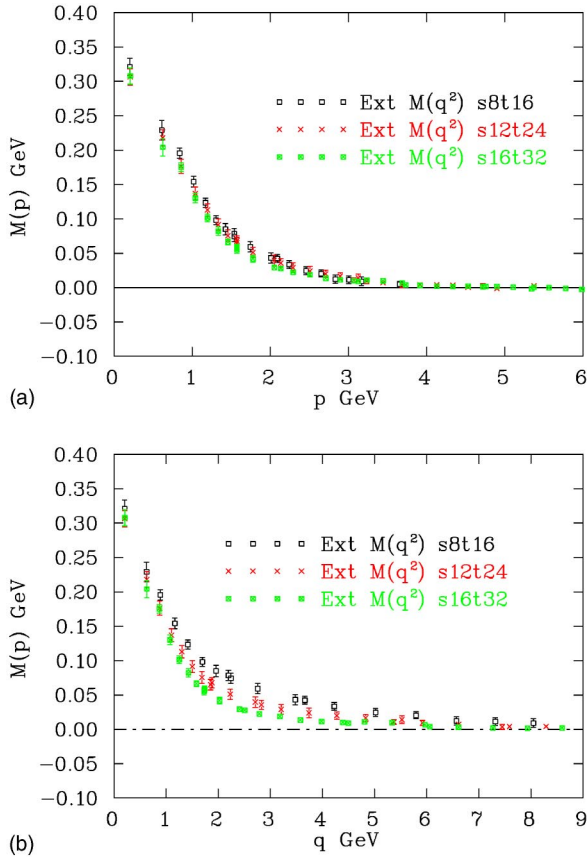
FIG. 4. The mass function $M(p)$ from a linear extrapolation to the chiral limit is shown for our three lattices. In the upper part of the figure $M(p)$ is plotted against the discrete lattice momentum p, whereas in the lower part it is plotted against the kinematical momentum q. The results again suggest that we most rapidly approach the continuum limit by plotting $M(p)$ against p.

continuum, the asymptotic quark mass function has the form

$$M(p^2) \stackrel{p^2 \to \infty}{=} -\frac{4\pi^2 d_M}{3} \frac{\langle \bar{\psi}\psi \rangle}{[\ln(\mu^2/\Lambda_{QCD}^2)]^{d_M}}$$

$$\times \frac{[\ln(p^2/\Lambda_{QCD}^2)]^{d_M-1}}{p^2} \qquad (18)$$

[see Ref. [19], Eq. (6.15)] where the anomalous dimension of the quark mass is $d_M = 12/(33 - 2N_f)$ for N_f quark flavors ($N_f = 0$ in the present case). The dependence of $M(p^2)$ on
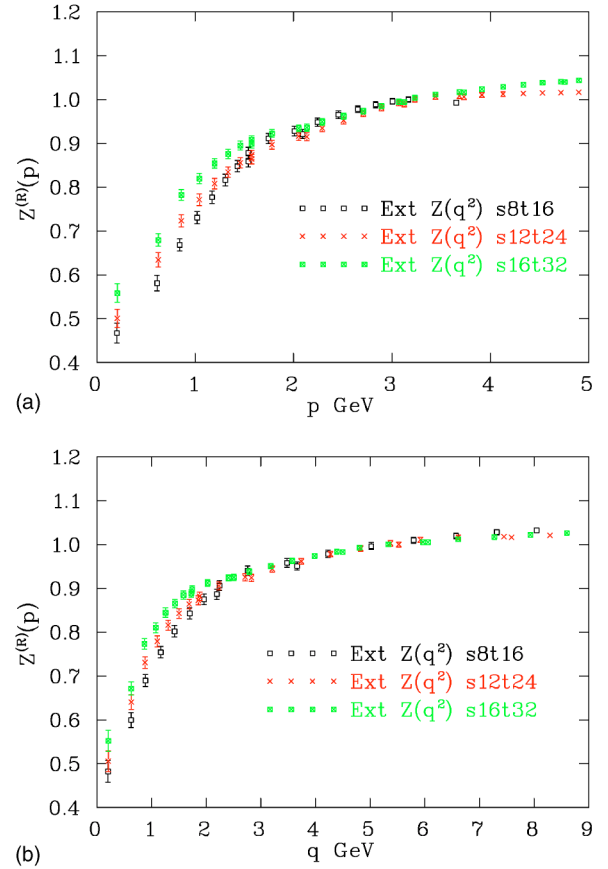

FIG. 5. The momentum-dependent wave-function renormalization function $Z^{(R)}(p) \equiv Z(\zeta^2; p)$ for renormalization point $\zeta = 3.44$ GeV in the p-scale and $\zeta = 5.31$ GeV in the q-scale from a linear extrapolation to the chiral limit. In the upper part of the figure, $Z^{(R)}(p)$ is plotted against the discrete lattice momentum p whereas in the lower part it is plotted against the kinematical momentum q. The results again suggest that we most rapidly approach the continuum limit by plotting $Z^{(R)}(p)$ against q.

the renormalization point μ is canceled by the dependence of the condensate, maintaining the renormalization point invariance of the mass function. We fit this form to the lattice data obtained by both linear and quadratic chiral extrapolation. A quadratic extrapolation was used on the AsqTad data [6] so it is useful for comparing with those results. Some results are presented in Table II.

The difference between the quadratic and linear extrapolations is no great surprise as our quark masses are rather heavy. This is a constraint of the volume. The relevant point

TABLE II. Extracted values of the quark condensate $\langle \bar{\psi}\psi \rangle$.

β	extrapolation	p fit region (GeV)	$-\langle \bar{\psi}\psi \rangle^{1/3}$ (MeV)	q fit region (GeV)	$-\langle \bar{\psi}\psi \rangle^{1/3}$ (MeV)
4.60	linear	3.6–4.5	337(39)	4.3–8.6	621(49)
4.60	quadratic	3.6–4.5	292(56)	4.3–8.6	575(72)
4.80	linear	3.6–5.3	327(22)	5.5–11.4	499(34)
4.80	quadratic	3.6–5.3	259(36)	5.5–11.4	395(54)

is that there is good agreement between the two lattices when p is the momentum, but not when q is the momentum.

IV. SUMMARY AND OUTLOOK

The momentum space quark propagator has been calculated in Landau gauge on three lattices with different lattice spacing a, but very similar physical volumes in order to explore the approach to the continuum limit. We calculated the nonperturbative momentum-dependent wave-function renormalization $Z(\zeta^2; p)$ and the nonperturbative mass function $M(p)$ for a variety of bare quark masses. We also explored the quark propagator in the chiral limit. As previously anticipated [8], the continuum limit for $Z(\zeta^2; p)$ is approached most rapidly when it is plotted against the kinematical lattice momentum q, whereas for the quark mass function $M(p)$, we have found that using the discrete lattice momentum p provides the most rapid approach to the continuum limit.

Future work should test our conclusions and further explore the continuum limit with one or more additional finer-lattice spacings. In addition, it will be necessary to use both finer and larger volume lattices, in particular to study the infrared behavior of $Z(\zeta^2, q)$. One can also use other kernels in the overlap fermion formalism, e.g., using a fat-link irrelevant clover action [21] as the overlap kernel [22,23] in order to further establish the robustness of our conclusions and to provide more accurate data. These studies are currently underway and results will be reported elsewhere.

ACKNOWLEDGMENTS

[1] C.W. Bernard, D. Murphy, A. Soni, and K. Yee, Nucl. Phys. B (Proc. Suppl.) **17**, 593 (1990).

[2] C.W. Bernard, A. Soni, and K. Yee, Nucl. Phys. B (Proc. Suppl.) **20**, 410 (1991).

[3] J.I. Skullerud and A.G. Williams, Phys. Rev. D **63**, 054508 (2001); Nucl. Phys. B (Proc. Suppl.) **83**, 209 (2000).

[4] J. Skullerud, D.B. Leinweber, and A.G. Williams, Phys. Rev. D **64**, 074508 (2001).

[5] P.O. Bowman, U.M. Heller, and A.G. Williams, Phys. Rev. D **66**, 014505 (2002).

[6] P.O. Bowman, U.M. Heller, D.B. Leinweber, and A.G. Williams, Nucl. Phys. B (Proc. Suppl.) **119**, 323 (2003).

[7] T. Blum *et al.*, Phys. Rev. D **66**, 014504 (2002).

[8] F.D.R. Bonnet, P.O. Bowman, D.B. Leinweber, A.G. Williams, and J.B. Zhang, Phys. Rev. D **65**, 114503 (2002).

[9] J.B. Zhang, F.D.R. Bonnet, P.O. Bowman, D.B. Leinweber, and A.G. Williams, Nucl. Phys. B (Proc. Suppl.) **119**, 831 (2003).

[10] R. Narayanan and H. Neuberger, Nucl. Phys. **B443**, 305 (1995).

[11] H. Neuberger, Phys. Lett. B **427**, 353 (1998).

[12] R.G. Edwards, U.M. Heller, and R. Narayanan, Phys. Rev. D **59**, 094510 (1999).

[13] D.B. Leinweber, J.I. Skullerud, A.G. Williams, and C. Parrinello, Phys. Rev. D **60**, 094507 (1999); **61**, 079901(E) (2000); D.B. Leinweber, J.I. Skullerud, A.G. Williams, and C.

Parrinello, *ibid.* **58**, 031501 (1998).

[14] F.D.R. Bonnet, P.O. Bowman, D.B. Leinweber, A.G. Williams, and J.M. Zanotti, Phys. Rev. D **64**, 034501 (2001); F.D.R. Bonnet, P.O. Bowman, D.B. Leinweber, and A.G. Williams, *ibid.* **62**, 051501(R) (2000).

[15] M. Lüscher and P. Weisz, Commun. Math. Phys. **97**, 59 (1985).

[16] F.D.R. Bonnet, D.B. Leinweber, A.G. Williams, and J.M. Zanotti, "Symanzik improvement in the static quark potential," hep-lat/9912044.

[17] F.D.R. Bonnet, P.O. Bowman, D.B. Leinweber, A.G. Williams, and D.G. Richards, Aust. J. Phys. **52**, 939 (1999).

[18] J. van den Eshof *et al.*, Comput. Phys. Commun. **146**, 203 (2002); Nucl. Phys. B (Proc. Suppl.) **106**, 1070 (2002).

[19] C.D. Roberts and A.G. Williams, Prog. Part. Nucl. Phys. **33**, 477 (1994).

[20] R. Alkofer and L. von Smekal, Phys. Rep. **353**, 281 (2001).

[21] CSSM Lattice Collaboration, J.M. Zanotti *et al.*, Phys. Rev. D **65**, 074507 (2002).

[22] W. Kamleh, D. Adams, D.B. Leinweber, and A.G. Williams, Nucl. Phys. B (Proc. Suppl.) **109**, 81 (2002); Phys. Rev. D **66**, 014501 (2002).

[23] W. Kamleh, D.J. Kusterer, D.B. Leinweber, and A.G. Williams, Nucl. Phys. B (Proc. Suppl.) **119**, 828 (2003).

[24] This is merely an illustrative example. See Ref. [8] for details on how these functions are actually calculated.